

Diffusion-limited kinetics of terrace growth on GaAs(110)

P. Piercy and A. M.-J. Castonguay

Department of Physics, University of Ottawa, Ottawa, Ontario, Canada K1N 6N5

(Received 30 July 2004; revised manuscript received 13 July 2005; published 19 September 2005)

The kinetics of thermal annealing of surface roughness created by low-energy ion bombardment of GaAs(110) is characterized *in situ* by a low-energy electron diffraction (LEED) spot profile analysis to investigate the underlying diffusion mechanisms involved. The coarsening of the step-and-terrace structure on the partially annealed surface is observed, showing power-law growth of the average terrace width $l \sim t^\beta$ with an exponent $\beta=0.23-0.26$ over two orders of magnitude in annealing time t in the temperature range 660–740 K. However, the terrace height distribution is shown to vary little with annealing, providing evidence for an Ehrlich-Schwoebel barrier at step edges. The LEED analysis also detects an additional, low amplitude height distribution contributing an interface width of less than 0.03 nm, which is interpreted as elastic deformation around subsurface defects and exhibits much slower relaxation kinetics during annealing than the terrace growth.

DOI: 10.1103/PhysRevB.72.115420

PACS number(s): 68.35.Ct, 61.14.Hg, 68.35.Fx

I. INTRODUCTION

Time-resolved measurements of annealing kinetics of nonequilibrium surface morphologies may be used to characterize atomic diffusion processes at surfaces. In spite of the long history of this field,^{1,2} there is still a great deal of room for both experimental and theoretical work to map out the kinetics of surface annealing, as a step towards a more predictive approach to the preparation and modification of surface nanostructures by either epitaxial growth or etching.³⁻⁶ In general, the kinetics of surface smoothing depends not only on material and thermodynamic parameters, but also on the initial surface morphology which may be far from equilibrium. The relaxation kinetics of specifically prepared surface structures such as ripples or mounds have been measured, and interpreted in terms of theoretical models for the evolution of the island morphology, to characterize the relevant diffusion processes involved.⁷⁻¹¹ The decay and coarsening of two-dimensional (2D) islands have been characterized on different surfaces,¹² as well as the equilibration of the terrace width distribution on a vicinal substrate.^{13,14} In addition, the thermal smoothing of surfaces roughened by either atom deposition during crystal growth or atom removal by ion bombardment has been analyzed using diffraction techniques.¹⁵⁻²⁰

Since epitaxial growth on GaAs(110) is of some interest for nanostructure fabrication, conditions for growth of flat and patterned surface morphologies have been studied,²¹ and the diffusion kinetics on this surface plays an important role. In the past decade, the effects of elevated substrate temperature on kinetic roughening of the GaAs(110) surface during low-energy ion bombardment have been characterized by scanning tunnel microscopy (STM).²² Recently, post-growth annealing of the GaAs(110) growth front in molecular beam epitaxy (MBE) has been shown to cause dramatic smoothing.²³

In this paper, we study the kinetics of thermal annealing of a GaAs(110) surface on the nanometer length scale at 575–740 K in vacuum, after using low-energy ion bombardment at room temperature to provide a disordered initial con-

dition, as described in Sec. II. It is well known that ion bombardment of GaAs causes subsurface sputter damage that remains after annealing,^{6,24} which is detected here by low-energy electron diffraction (LEED) as a low-amplitude height distribution at the surface, in addition to the step-and-terrace structure. In Sec. III, the theory needed to distinguish these two types of height defect is outlined. In Sec. IV, the interface width due to both are determined, while the time evolution of the average terrace width on the surface and its temperature dependence is shown in Sec. V. These results are compared with existing theoretical models and experiments on other systems in Sec. VI, and the surface annealing mechanisms in our experimental conditions are discussed.

II. EXPERIMENTAL SETUP AND SAMPLE PREPARATION

The experiments were performed in an ultrahigh vacuum chamber with a base pressure below 10^{-10} Torr and equipped with surface analysis instruments for low-energy electron-diffraction spot profile analysis (SPA-LEED)²⁵ and Auger electron spectroscopy (AES), as described previously.¹⁹

Gallium arsenide wafers purchased²⁶ with polished (110) surface oriented with an accuracy of 0.5° were cut to a sample size of about 12×12 mm². The sample was mounted on a molybdenum holder with backing plate heated from behind by a tungsten filament. The sample temperature was monitored by chromel-alumel thermocouples spot welded to the sample holder and controlled automatically.¹⁸ (The measurement accuracy of the sample temperature is about ± 25 K, after taking into account the steady-state temperature difference between the sample and holder, using a rough estimate made afterwards by replacing the sample with a molybdenum plate of the same size with a thermocouple welded to it directly.) Initially, the sample was cleaned *ex situ* by rinsing in methanol, and in ultrahigh vacuum by argon ion sputtering at an ion energy of 500 eV at room temperature, after which the sample appears amorphous, i.e., no LEED pattern was observed until subsequent annealing to above 450 K.

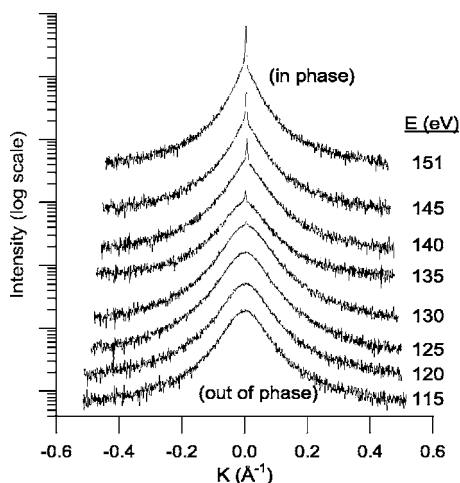


FIG. 1. Profiles of (0, 0) diffraction spot for electron energies ranging from an out-of-phase condition to an in-phase condition with respect to single height steps.

A rough initial surface for annealing studies was prepared by argon-ion bombardment at normal incidence at an energy of 230 eV. Although qualitatively similar results were found at 500 eV, the lower energy was used to reduce subsurface damage.²⁴ The ion beam was defocused to give a more uniform incident ion flux over the region of the sample monitored by the LEED beam with width of ≈ 1 mm. The ion flux of $\approx 3 \mu\text{A}/\text{cm}^2$ for 20 min is estimated to remove roughly 20 monolayers (MLs), to within a factor of 2, using the sputter yield data given for different conditions in Refs. 24,27,28. However, the relative ion dose was controlled to within a few percent, resulting in a reproducible surface preparation, as observed after annealing.

It has been shown elsewhere by AES that, after sputtering at low ion energies with ion flux similar to ours, the near-surface region becomes arsenic deficient, but annealing to 800 K caused substantial recovery of the initial stoichiometry.²⁹ However, surface degradation associated with arsenic desorption has been observed by scanning tunnel microscopy to begin at a temperature in the range 775–800 K.³⁰ Our rough AES data is consistent with this, and gives a peak intensity ratio Ga(1070 eV)/As(1228 eV) after sputtering that was $\approx 7\% \pm 4\%$ higher than after subsequent annealing to 660–740 K; annealing to lower temperatures below 575 K did not show recovery towards stoichiometry, above the noise in our data. Experiments were restricted to temperatures ≤ 740 K to avoid thermal desorption of As. After sputtering and annealing, no impurities could be seen on the surface with AES above the noise level of 1%, except for embedded argon giving an Ar(214 eV) signal level of $< 10\%$ of the low-energy peaks from gallium and arsenic combined.

III. DIFFRACTION SPOT PROFILES—EFFECTS OF TWO HEIGHT DEFECTS

A sample set of LEED spot profiles measured on the (0,0) diffraction spot is shown in Fig. 1. Although the scans shown were taken in the [001] direction, the 2D spot profiles were

very nearly isotropic—the spot width varied by less than 10% vs direction in k space. These measurements were performed at room temperature after sputter roughening at 300 K as described above, followed by annealing at 735 K for 5 min. The energies of the different scans were chosen to give perpendicular momentum transfer $\hbar k_{\perp}$ in the range $k_{\perp}d = 7\pi - 8\pi$, where $d = 2.00 \text{ \AA}$ is the atomic step height. At $E = 115$ eV, $k_{\perp}d = 7\pi$ gives an out-of-phase condition for electron scattering between terraces separated by a single step height; the step and terrace structure has maximal effect on the spot profile at this energy, and the width of the spot profile is related to the inverse of the average terrace width on the surface.³¹ At $E = 151$ eV, $k_{\perp}d = 8\pi$ gives an in-phase condition, at which the diffraction profile is not affected by a perfect step-and-terrace structure. The trend shown in Fig. 1 was observed qualitatively to repeat over a wider energy range covering other in- and out-of-phase conditions as well.

The LEED diffraction spot profile at a crystalline surface with two types of height defects may be described in the kinematical approximation by a structure factor $S(\vec{k})$ defined as the squared modulus of the 2D Fourier transform of the surface height function $\sigma(\vec{r}_{\parallel}) = e^{ik_{\perp}z(\vec{r}_{\parallel})}$.^{31,32} The surface height z at lateral position \vec{r}_{\parallel} has two contributions, $z(\vec{r}_{\parallel}) = h(\vec{r}_{\parallel}) + \delta h(\vec{r}_{\parallel})$, where a step-and-terrace structure is described by the surface height $h(\vec{r}_{\parallel})$ which is an integer multiple of the atomic step height d , and $\delta h(\vec{r}_{\parallel})$, which describes a small, continuous height distribution.

In the analysis, we assume that the two effects are statistically independent. This is supported by the observation that the average terrace width is smaller, and grows much faster, than the correlation range of $\delta h(\vec{r}_{\parallel})$ as found in Sec. IV A and V. Then the structure factor $S(\vec{k})$ reduces to a 2D convolution of the structure factor $S_h(\vec{k})$ due to an otherwise-perfect step-and-terrace structure and $S_{\delta h}(\vec{k})$ due to δh alone. Both $S_h(\vec{k})$ and $S_{\delta h}(\vec{k})$ decompose independently into a sum of a Bragg peak of the form $G_{\alpha}(k_{\perp})\delta(\vec{K})$ plus a broad, diffuse profile component $S_{\alpha}^{\text{diff}}(k_{\perp}, \vec{K})$ where α refers to the h or δh factor, and k_{\perp} and \vec{K} are components of \vec{k} perpendicular and parallel to the surface, respectively. The structure factor therefore separates into two terms as

$$S(\vec{k}) = G_h(k_{\perp})G_{\delta h}(k_{\perp})\delta(\vec{K}) + S^{\text{diff}}(k_{\perp}, \vec{K}) \quad (1)$$

shown here for the (0,0) diffraction spot only. The delta-function term is broadened slightly by the resolution of the diffraction instrument, giving a narrow spike with full width at half maximum (FWHM) $\approx 0.005 \text{ \AA}^{-1}$ as seen near the in-phase condition in Fig. 1. The diffuse component in the spot profile, $S^{\text{diff}}(k_{\perp}, \vec{K})$, is discussed in Sec. V.

Finally, we note that the STM data of Pechman, Wang, and Weaver³⁰ shows double-height steps occurring occasionally. Although our diffraction data is dominated by the effects of single-height steps, the coexistence of a small concentration of double-height steps cannot be ruled out.

IV. SURFACE HEIGHT DISTRIBUTION

The interface width (i.e., the standard deviation of the surface height distribution) receives contributions from both

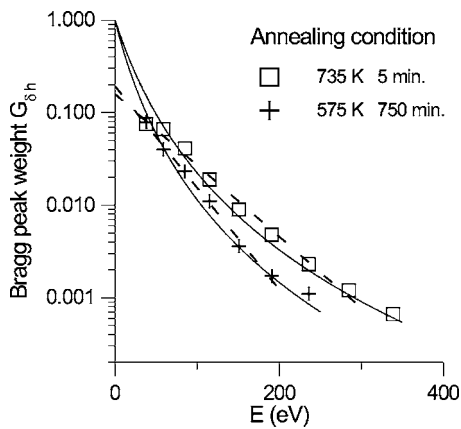


FIG. 2. Relative weight $G_{\delta h}$ of Bragg peak measured at in-phase conditions corresponding to electron energies E , after two different annealing conditions given.

the step-and-terrace morphology as well as from other defects causing a low-amplitude, continuous height variation in addition. Although the former contribution dominates over the latter in the overall interface width, each contribution may be measured separately, as described below.

A. Low amplitude roughness

After the sputtering and annealing preparation described in Sec. II, diffraction spot profiles were measured for a range of energies corresponding to in-phase conditions, showing a Bragg peak intensity that decreases with increasing energy. At in-phase conditions, a perfect step-and-terrace structure does not alter the diffraction profiles which are therefore described by the structure factor $S_{\delta h}(\vec{k})$ due to other defects alone. Then the relative weight of the Bragg peak, measured as the fraction of its integrated intensity in the full 2D spot profile, gives just $G_{\delta h}(k_{\perp})$ and is plotted on a log scale in Fig. 2 as a function of LEED energy E . (The 2D integration of the LEED intensity in k space was done by fitting the spot profiles in $[1\bar{1}0]$ and $[001]$ directions to a sum of a narrow Gaussian plus a broad 2D Lorentzian line shape plus a constant background, and then assuming an isotropic profile to do the integrals numerically in two dimensions.)

The continuously decreasing graph over two orders of magnitude in $G_{\delta h}$ provides evidence for a continuous distribution of surface height. Only atomic displacements perpendicular to the surface are detected in Fig. 2, in which data from both the $(0, 0)$ and $(0, 1)$ beams are included and fall on the same lines. (The $(0, 1)$ beam is not very sensitive to small lateral displacements since $K_{(0,1)} \approx 1.1 \text{ \AA}^{-1}$ along $[001]$ is much less than k_{\perp} which is $\approx 11 \text{ \AA}^{-1}$ at an energy of 115 eV. The in-phase conditions for the $(0, 1)$ beam are at energies coinciding nearly with out-of-phase conditions for the $(0, 0)$ beam, due to crystal symmetry.)

The contribution to the interface width due to this continuous height perturbation alone is estimated to be less than 0.3 \AA . This is seen by comparing the data in Fig. 2 with a gamma distribution of surface heights for example, with probability function $p_n(\delta h) \propto (\delta h)^n e^{-\delta h/\sigma}$ giving $G_{\delta h} = (1$

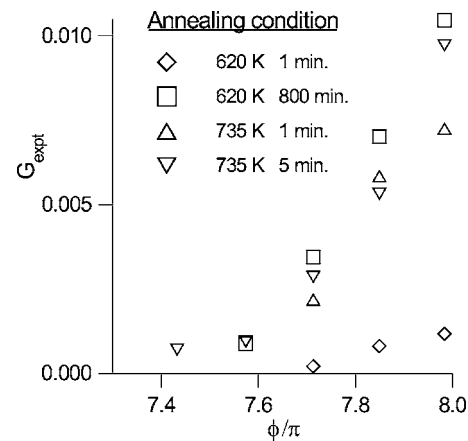


FIG. 3. Measured weight G_{expt} of Bragg peak versus phase factor $\phi = k_{\perp} d$, after four different annealing conditions given.

$+k_{\perp}^2 \sigma^2)^{-(n+1)}$.³³ This gives a rough fit to the $G_{\delta h}(E)$ data for $n=4$, as shown by the solid lines in the figure, with interface width of 0.28 \AA after annealing at 575 K for 750 min, and 0.25 \AA after 735 K for 5 min. On the other hand, the nearly linear decrease in $\ln G_{\delta h}$ vs E (or k_{\perp}^2) in Fig. 2 is somewhat suggestive of a Gaussian height distribution, for which one expects $\ln G_{\delta h}(k_{\perp}) = -w^2 k_{\perp}^2$.³² The interface width determined from the slopes of the dashed lines in Fig. 2 is 0.16 \AA after annealing at 575 K for 750 min, and 0.13 \AA after annealing at 735 K for 5 min. However, in this scenario the observed intercept, $G_{\delta h} \rightarrow 0.2$ (rather than 1) as $E \rightarrow 0$, would have to be attributed to other surface defects. (The thermal Debye-Waller factor makes only a minor contribution.)

The lateral correlation length of $\delta h(\vec{r}_{\parallel})$ is related to the inverse width of the spot profile $S_{\delta h}^{\text{diff}}(\vec{K})$ at in-phase conditions, in the limiting case $wk_{\perp} \ll 1$.³² Extrapolating from sample measurements of the spot width versus in-phase-condition energies down to 38 eV, we roughly estimate the correlation length (as $2/\text{HWHM}$) to be on the order of 100 \AA . We did not detect a significant evolution of the lateral correlation length; the diffraction spot width measured at 59 eV on the $(1, 0)$ spot was practically constant vs annealing time at 705 K.³⁴

B. Terrace height distribution due to steps

The rapid decrease of the Bragg peak intensity as the electron energy is adjusted away from an in-phase condition, as seen qualitatively in Fig. 1, may be understood in terms of a step-and-terrace morphology. The relative weight G_{expt} of the Bragg peak is calculated as above, but over the range of energy in Fig. 1, corresponding to phase factor $\phi = k_{\perp} d = 7\pi - 8\pi$. Only the range $E = 130 - 151 \text{ eV}$, or $\phi = 7.4\pi - 8\pi$, is shown in Fig. 3 as the Bragg peak was too small to detect otherwise.

In Fig. 3, the value of G_{expt} is already very small at the in-phase condition $\phi = 8\pi$ (or 151 eV), due to other defects as described in the previous section. According to Eq. (1), we let $G_{\text{expt}}(\phi) = G_h(\phi) G_{\delta h}(\phi)$. Since G_{expt} in Fig. 3 changes much more rapidly with ϕ (or E) than $G_{\delta h}$ in Fig. 2, we may

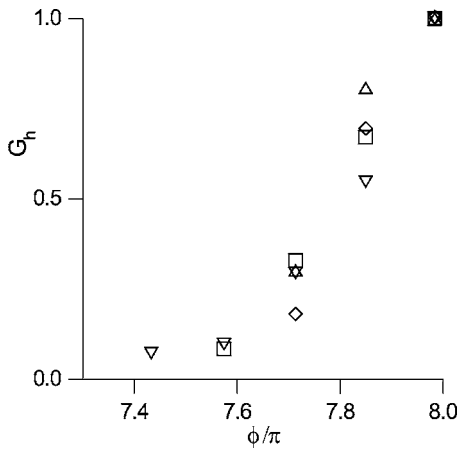


FIG. 4. Relative weight G_h due to step-and-terrace structure, obtained by normalization of data in Fig. 3, as described in the text. The symbols correspond to the same annealing conditions as in Fig. 3.

approximate $G_{\text{expt}}(\phi) \approx G_h(\phi)G_{\delta h}(8\pi)$ over the small range of ϕ in Fig. 3.

The results for $G_h(\phi)$ are shown in Fig. 4. The data for four different annealing conditions overlap, within measurement noise, indicating that the terrace height distributions are approximately the same, after the different annealing temperatures and times given in Fig. 3. Specifically, the fractional surface areas $\{\theta_n\}$ at heights $h=nd$ are determined from Fig. 4 by fitting to $G_h(\phi) = |\sum_{n=1}^N \theta_n e^{i\phi n}|^2$,³¹ where we truncate the sum at $N=5$ and also require $\sum_{n=1}^N \theta_n = 1$. The coverages $\{\theta_n\}$ vary by only $\pm 5\%$ between data sets, which is certainly within the limits of accuracy of this analysis and data. The average of the results for the four data sets gives $\{\theta_1, \dots, \theta_5\} = 0.21, 0.29, 0.24, 0.16, 0.10$ ML. The interface widths calculated from the individual terrace height distributions are in the range $w = 1.1 - 1.3$ ML.

V. GROWTH OF THE AVERAGE TERRACE WIDTH DURING ANNEALING

The surface was initially roughened by sputtering at room temperature as described in Sec. II. This was followed by a short pre-annealing stage at 510 K for 10 min which gave a (1×1) pattern of broad diffraction spots. Then time-resolved SPA-LEED experiments were performed while the sample was annealed further at 575–735 K for up to 13 h. The intensity profile of the $(0,0)$ diffraction spot at the out-of-phase condition at $E=115$ eV was measured repeatedly in $[1\bar{1}0]$ and $[001]$ directions across the Brillouin zone and automatically recorded, as described in Ref. 18. To determine the width of the spot profile, which shows only a diffuse component, the diffraction spot profile was fitted to a Lorentzian line shape plus a constant background. During annealing, the width of the diffuse profile decreased with time, as shown in Fig. 5, indicating an increase in the average terrace width.

However, the diffuse spot profile measured at an out-of-phase condition receives contributions from both the terrace width distribution and the low-amplitude roughness de-

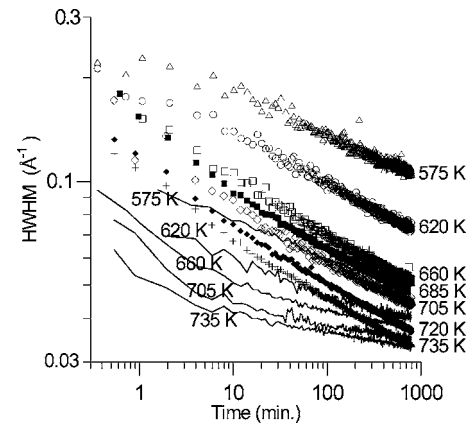


FIG. 5. Diffraction spot width (HWHM) vs time at annealing temperatures shown. Data at the out-of-phase condition $E = 115$ eV are plotted as points; solid lines are data at the in-phase condition $E=151$ eV.

scribed in Sec. IV A. At an out-of-phase condition, the profile S^{diff} may be approximated as the convolution of just the diffuse parts of S_h and $S_{\delta h}$, that is,

$$S^{\text{diff}}(k_{\perp}, \vec{K}) \approx \int dK' S_h^{\text{diff}}(k_{\perp}, \vec{K} - \vec{K}') S_{\delta h}^{\text{diff}}(k_{\perp}, \vec{K}'). \quad (2)$$

This is valid provided the Bragg peak delta function contributes little to the integrated intensity of the 2D spot profile $S_{\delta h}$. This is indeed the case here, as shown by Figs. 1 and 2.

We may approximate $S_{\delta h}$ by the spot profile at the in-phase condition at $E=151$ eV. The latter profile is fitted to a sum of a Gaussian line shape to model the narrow Bragg peak and a Lorentzian to model the diffuse profile component $S_{\delta h}^{\text{diff}}$. The width of $S_{\delta h}^{\text{diff}}$ determined this way is also shown in Fig. 5 (as solid lines) vs annealing time. Compared to the width of the measured profile S^{diff} at out-of-phase, the in-phase profile $S_{\delta h}^{\text{diff}}$ has a smaller width that varies more slowly with time.³⁵

The width of S_h^{diff} (due to the step-and-terrace structure alone) at the out-of-phase condition is determined from Eq. (2) by deconvolution. This was done approximately by assuming an isotropic 2D-Lorentzian form for both $S_h^{\text{diff}}(k_{\perp}, \vec{K})$ and $S_{\delta h}^{\text{diff}}(k_{\perp}, \vec{K})$, and using a numerically calculated look-up table to determine the width (HWHM) of S_h^{diff} from the widths of $S_{\delta h}^{\text{diff}}$ and S^{diff} , the measured profiles at the in-phase and out-of-phase conditions. This method is sufficiently accurate for most of the data range, for which the deconvolution reduces the spot width by 10–25%; the exception for very late times at higher temperatures is pointed out below. The average terrace width is calculated as $l = 2/\Gamma$ where Γ is the HWHM of S_h^{diff} determined in this way.

In Fig. 6, the growth of the average terrace width with annealing time is shown on a log-log plot, for various temperatures. The straight lines in the figure are fits to the power law $l \sim t^{\beta}$. For temperatures 660–735 K and $t \leq 100$ min, the exponent β falls in the range 0.23–0.26 with an average of 0.24, providing strong evidence for $t^{1/4}$ kinetics of terrace growth.

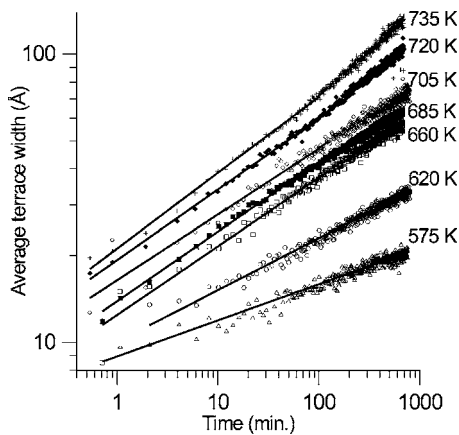


FIG. 6. Average terrace width vs annealing time at the temperatures given. Straight lines are power law fits to the data. Exponents given in the text.

For later times 100–800 min, the slopes are about 0.22 for 660–705 K data, increasing to 0.31 at 735 K, shown as dashed lines in Fig. 6. However, Fig. 5 shows that, at the higher temperatures 705–735 K, the spot profile widths at the out-of-phase condition exceed those at in-phase by only 60% or less at 100 min, and even less at later times. In this case the simple deconvolution procedure we used becomes less accurate, which may partly explain the different slopes seen in Fig. 6 at late times.

In comparison, the original experimental spot width in Fig. 5 evolves as $\Gamma \sim t^{-\beta}$ with $\beta \approx 0.20$ for times up to 30 min, followed by a smaller exponent at later times. The deconvoluted data in Fig. 6 shows scaling behavior extending to later times than seen in the raw data in Fig. 5.

In addition, the temperature dependence of the terrace width at fixed time may be parametrized by $l \sim (t/\tau)^\beta$ with $\tau^{-1} \propto e^{-E_a/kT}$ over temperatures 660–735 K, from which we determine the activation energy $E_a = 1.3$ eV ($\pm 10\%$), in complete agreement with Ref. 30.

At the lower temperatures of 575 and 620 K, the terrace width grows more slowly with $\beta = 0.12$ and 0.18, respectively. The kinetics may be affected by point defects remaining after sputtering; the stoichiometry of the near-surface region was not as fully annealed at these temperatures, as discussed in Sec. II.

VI. DISCUSSION

Two different characteristics of the surface morphology of GaAs(110) were studied by LEED spot profile analysis after low-energy ion bombardment and annealing. (i) The main feature is the atomic-height step-and-terrace structure that was described in Sec. IV B and V, which we discuss further below. (ii) In addition, a continuous height distribution was characterized in Sec. IV A, giving a small contribution to the interface width estimated to be in the range 0.1–0.3 Å. We attribute this to elastic deformation around near-surface defects such as vacancies, embedded argon atoms, or dislocations which are known to remain after ion bombardment and annealing of GaAs surfaces.^{6,24} The peak-to-peak surface

height variation due to this effect alone (i.e., ignoring steps) may be estimated as $4w \approx 0.5\text{--}1.2$ Å. This is of the size that could be expected above buried dislocations,³⁶ and is similar to that found previously on overlayers of Ge on Si(111),³⁷ for example. This surface distortion is correlated laterally over lengths of the order of magnitude of 100 Å, which is comparable with typical depths of sputter damage on GaAs for low-energy ions.^{6,24}

The step-and-terrace structure we observe after ion bombardment at room temperature followed by annealing at elevated temperature may be compared with that observed by STM by Wang, Pechman, and Weaver²² after high-temperature sputtering at a low ion flux on the GaAs(110) surface. Although in our experiments the surface is initially amorphous after sputtering at room temperature, some comparison may be made after annealing. We found from Fig. 4 that the terrace height distribution does not change significantly; the interface width was $w = 1.1\text{--}1.3$ MLs and varied negligibly compared to the growth of the average terrace width. This indicates restricted interlayer diffusion in our annealing experiments, suggestive of a Ehrlich-Schwoebel barrier at step edges, as found previously in the kinetic roughening experiments in Ref. 22. Although the average terrace width grows during annealing whereas it initially decreases with time to a steady-state value during sputtering, it may be pointed out that the step density found in Fig. 3 of Ref. 22 after sputter removal of just one or two monolayers at elevated temperature is similar to the average terrace width we find after annealing the same time at a similar temperature after initially sputtering at room temperature.

Although we determined an activation energy for mass transport on the surface of $E_a = 1.3$ eV, our results do not determine unambiguously the diffusion mechanism that this corresponds to. Different coarsening mechanisms predict $\beta = 1/4$ via diffusion either across terraces or along step edges. However, this activation energy coincides with that estimated in Ref. 30 from STM observations of the evolution of the vacancy island density due to terrace diffusion, which we assume dominates in our experiments as well.

On the other hand, the terrace widths we find after sputter-etching and annealing in vacuum appear to be much smaller than those observed in studies of epitaxial growth of GaAs on the cleaved (110) surface. Post growth annealing at 600°C in an As flux has been shown by Yoshita, Akiyama, Pfeiffer, and West²³ to give terrace widths on the order of μm . The formation of these large terrace widths was explained by the relatively low migration energy barrier for As and Ga adatom diffusion calculated to be 0.57–0.86 eV on this surface, with lower energies for motion along $[1\bar{1}0]$ than $[001]$.³⁸ This regime for post-growth annealing kinetics is clearly different from our case in vacuum after sputtering, for which we interpret the activation energy E_a as the sum of the energy for adatom detachment from a step edge plus the adatom migration energy on a terrace, consistent with the energetics of divacancy diffusion along $[1\bar{1}0]$ discussed in Ref. 30. In comparison, earlier calculations of diffusion of single As and Ga vacancies gave activation energies ≥ 1.5 eV depending on charge state and direction,^{39,40} and anisotropic diffusion induced by an STM tip has been observed.⁴¹ However, in our

experimental conditions we found an isotropic average terrace width after annealing.

The growth of the average terrace width $l \approx t^{1/4}$ observed on GaAs(110) during annealing at 660–735 K after sputtering is consistent with our previous study on the TiO₂ rutile (110) surface,^{18,19} for which the interface width stayed nearly constant at ≈ 1.0 ML after a similar sputter dose. The similarity between these two systems is noteworthy, in view of the different power laws found in other annealing experiments on different systems after either multilayer deposition or sputtering,^{16,17,20} for which the scaling law $l \sim t^\beta$ was found with exponents $\beta = 0.2-0.5$. For example, on the sputtered CdTe(001) surface, annealing after sputtering gave $\beta = 0.5$,²⁰ which was attributed to a barrier for attachment and detachment of atoms at step edges, clearly pointing to different activation energies controlling the kinetics in that case.

The terrace growth kinetics on GaAs(110) may be understood in terms of models for the coarsening of an array of two-dimensional islands. This is reasonable in view of the narrow and (roughly) constant terrace height distribution we found. Additional support for this approach is found in our past results on annealing the TiO₂(110) surface which

showed the same exponent after initial sputtering conditions removing 0.5 ML and 10–20 MLs.^{18,19} Step-edge fluctuations mediated by diffusion across terraces may lead to coarsening of the nearly 2D island morphology. In one extreme, island decay may occur by a pinch-off effect when opposite terrace edges meet, as seen elsewhere by STM on Cu and Ag(100) surfaces.⁴² This mechanism has been described theoretically, giving relaxation time $\tau \propto l^4$ for a parallel step array, created by a sinusoidal surface profile, for example.⁴³ The same exponent for coarsening, $\beta = 1/4$, is predicted due to diffusion of compact 2D islands leading to coalescence,⁴⁴ but this may be less representative of our surface morphology which we expect is a rather ramified 2D island structure during annealing, after sputter removal at room temperature for which diffusion is negligible; this assumption could be verified by scanning probe studies.

In either case, a crossover to asymptotic behavior given by Oswald ripening is expected theoretically, with exponent $\beta = 1/3$ given by Lifschitz-Slyosov theory in two dimensions.^{10,45} However, this was not observed over the range of average terrace widths 1–10 nm probed in our experiments.

-
- ¹C. Herring, J. Appl. Phys. **21**, 301 (1950).
²W. Mullins, J. Appl. Phys. **30**, 77 (1959).
³*Morphological Organization in Epitaxial Growth and Removal*, edited by Z. Zhang and M. Lagally (World Scientific, Singapore, 1998).
⁴A. Pimpinelli and J. Villain, *Physics of Crystal Growth* (Cambridge University Press, Cambridge, U.K., 1998).
⁵D. Cahill, J. Vac. Sci. Technol. A **21**, S110 (2003).
⁶J. Malherbe, Crit. Rev. Solid State Mater. Sci. **19**, 129 (1994).
⁷J. Blakely and C. Umbach, in *Diffusion at Interfaces, Microscopic Concepts*, edited by H. K. M. Grunze, and J. Weimer (Springer, Berlin, 1988), p. 102.
⁸S. J. Chey, J. E. VanNostrand, and D. G. Cahill, Phys. Rev. Lett. **76**, 3995 (1996).
⁹A. Ichimiya, K. Hayashi, E. D. Williams, T. L. Einstein, M. Uwaha, and K. Watanabe, Phys. Rev. Lett. **84**, 3662 (2000).
¹⁰M. Zinke-Allmang, L. Feldman, and M. Grabow, Surf. Sci. Rep. **16**, 377 (1992).
¹¹A. Pimpinelli, J. Villain, D. Wolf, J. Metois, J. Heyraud, I. Elkinani, and G. Uimin, Surf. Sci. **295**, 143 (1993).
¹²M. Giesen, Prog. Surf. Sci. **68**, 1 (2001).
¹³H.-C. Jeong and E. Williams, Surf. Sci. Rep. **34**, 171 (1999).
¹⁴N. Bartelt, J. Goldberg, T. Einstein, and E. Williams, Surf. Sci. **273**, 252 (1992).
¹⁵H. J. Ernst, F. Fabre, and J. Lapujoulade, Phys. Rev. Lett. **69**, 458 (1992).
¹⁶J.-K. Zuo and J. F. Wendelken, Phys. Rev. Lett. **70**, 1662 (1993).
¹⁷H.-N. Yang, G.-C. Wang, and T.-M. Lu, Phys. Rev. Lett. **74**, 2276 (1995).
¹⁸B. Grossmann and P. Piercy, Phys. Rev. Lett. **74**, 4487 (1995).
¹⁹A. Cai and P. Piercy, Phys. Rev. B **66**, 115414 (2002).
²⁰H. Neureiter, S. Schinzer, M. Sokolowski, and E. Umbach, J. Cryst. Growth **201/202**, 93 (1999).
²¹P. Tejedor, P. Smilauer, C. Roberts, and B. A. Joyce, Phys. Rev. B **59**, 2341 (1999).
²²X. Wang, R. Pechman, and J. Weaver, Surf. Sci. Lett. **364**, L511 (1996).
²³M. Yoshita, H. Akiyama, L. Pfeiffer, and K. West, Jpn. J. Appl. Phys., Part 2 **40**, L252 (2001).
²⁴S. Pearton, U. Chakrabarti, A. Perley, and K. Jones, J. Appl. Phys. **68**, 2760 (1990).
²⁵U. Scheithauer, G. Meyer, and M. Henzler, Surf. Sci. **178**, 441 (1986).
²⁶Princeton Scientific Corp., Princeton, NJ.
²⁷J. Malherbe, Crit. Rev. Solid State Mater. Sci. **19**, 55 (1994).
²⁸X. Wang, R. Pechman, and J. Weaver, J. Vac. Sci. Technol. B **13**, 2031 (1995).
²⁹H. Gnaser, B. Heinz, W. Bock, and H. Oechsner, Phys. Rev. B **52**, 14086 (1995).
³⁰R. J. Pechman, X. S. Wang, and J. H. Weaver, Phys. Rev. B **51**, 10929 (1995).
³¹R. Altsinger, H. Busch, M. Horn, and M. Henzler, Surf. Sci. **200**, 235 (1988).
³²H.-N. Yang, G.-C. Wang, and T.-M. Lu, *Diffraction from Rough Surfaces and Dynamic Growth Fronts* (World Scientific, Singapore, 1993).
³³Y.-P. Zhao, G.-C. Wang, and T.-M. Lu, Phys. Rev. B **55**, 13938 (1997).
³⁴P. Piercy (unpublished).
³⁵The time dependence of the width of the spot profile at the in-phase condition $E = 151$ eV depends on higher moments of the continuous height distribution $\delta h(\vec{r}_\parallel)$ since $k_\perp^2 \langle \delta h^2 \rangle > 1$ and does not reflect the evolution of the correlation length alone (Ref. 32).
³⁶F. R. N. Nabarro, *Theory of Crystal Dislocations* (Clarendon Press, Oxford, 1967).
³⁷M. H. von Hoegen, A. Al-Falou, H. Pietsch, B. Muller, and M. Henzler, Surf. Sci. **298**, 29 (1993).
³⁸A. Ishii, T. Aisaka, J.-W. Oh, M. Yoshita, and H. Akiyama, Appl.

- Phys. Lett. **83**, 4187 (2003).
- ³⁹J. Y. Yi, J. S. Ha, S. J. Park, and E. H. Lee, Phys. Rev. B **51**, 11198 (1995).
- ⁴⁰G. Lengel, M. Weimer, J. Gryko, and R. Allen, J. Vac. Sci. Technol. A **12**, 1855 (1994).
- ⁴¹G. Lengel, J. Harper, and M. Weimer, Phys. Rev. Lett. **76**, 4725 (1996).
- ⁴²W. W. Pai, J. F. Wendelken, C. R. Stoldt, P. A. Thiel, J. W. Evans, and D. J. Liu, Phys. Rev. Lett. **86**, 3088 (2001).
- ⁴³J. Erlebacher and M. Aziz, Surf. Sci. **374**, 427 (1997).
- ⁴⁴D. Sholl and R. Skodje, Physica A **231**, 631 (1996).
- ⁴⁵A. Lo and R. Skodje, J. Chem. Phys. **112**, 1966 (2000).